Annals of Glaciology

Paper

Cite this article: Riverman KL, Anandakrishnan S, Alley RB, Holschuh N, Dow CF, Muto A, Parizek BR, Christianson K, Peters LE (2019). Wet subglacial bedforms of the NE Greenland Ice Stream shear margins. *Annals of Glaciology* **60**(80), 91–99. https://doi.org/10.1017/aog.2019.43

Received: 1 July 2019
Revised: 19 November 2019
Accepted: 20 November 2019
First published online: 18 December 2019

Keywords:
Ice streams; seismics; subglacial sediments; moraine formation

Author for correspondence:
Kiya L. Riverman, E-mail: kiyar@uoregon.edu

© The Author(s) 2019. This is an Open Access article, distributed under the terms of the Creative Commons Attribution licence (http://creativecommons.org/licenses/by/4.0/), which permits unrestricted re-use, distribution, and reproduction in any medium, provided the original work is properly cited.

cambridge.org/aog

Wet subglacial bedforms of the NE Greenland Ice Stream shear margins

Kiya L. Riverman[1], Sridhar Anandakrishnan[2], Richard B. Alley[2], Nicholas Holschuh[3,4], Christine F. Dow[5], Atsuhiro Muto[6], Byron R. Parizek[2,7], Knut Christianson[3] and Leo E. Peters[8]

[1]Department of Earth Sciences, University of Oregon, Eugene, OR, USA; [2]Department of Geosciences, and Earth and Environmental Systems Institute, Pennsylvania State University, University Park, PA, USA; [3]University of Washington, Seattle, WA, USA; [4]Amherst College, Amherst, MA; [5]University of Waterloo, Waterloo, ON, Canada; [6]Temple University, Pittsburgh, PA, USA; [7]Geosciences and Mathematics, Pennsylvania State University, DuBois, PA, USA and [8]Seismic Research Centre, University of the West Indies, St. Augustine, Trinidad

Abstract

We describe elongate, wet, subglacial bedforms in the shear margins of the NE Greenland Ice Stream and place some constraints on their formation. Lateral shear margin moraines have been observed across the previously glaciated landscape, but little is known about the ice-flow conditions necessary to form these bedforms. Here we describe in situ sediment bedforms under the NE Greenland Ice Stream shear margins that are observed in active-source seismic and ground-penetrating radar surveys. We find bedforms in the shear margins that are ~500 m wide, ~50 m tall, and elongated nearly parallel to ice-flow, including what we believe to be the first subglacial observation of a shear margin moraine. Acoustic impedance analysis of the bedforms shows that they are composed of unconsolidated, deformable, water-saturated till. We use these geophysical observations to place constraints on the possible formation mechanism of these subglacial features.

Introduction

Bedforms are thought to form preferentially where ice flows rapidly over deformable sediments. Observations of formerly glaciated landscapes in marine and terrestrial settings reveal widespread subglacial bedforms (e.g., Menzies, 1989; Clark, 2010; King and others, 2016). Despite the ubiquity of bedforms, few unifying theories of their formation have emerged. One major limitation to further model development is that relatively few studies have observed bedforms in situ beneath actively flowing ice (Smith, 1997; Clarke and others, 2000; Smith and others, 2007; King and others, 2009, 2016). As a result, little is known of the ice-flow and subglacial conditions necessary to form and preserve till bedforms.

Subglacial bedforms associated with shear margins are of particular interest because of their potential role in influencing shear margin movement and stability. Ice generally enters ice streams through tributary flow or by flowing across shear margins. These shear margins often support very high shear stresses (>100 kPa), which may represent a large component (50–100%) of the driving stress for the entire ice stream (Van der Veen and others, 2007). As such, there is much interest in studying processes associated with shear margin position and stability (Hindmarsh and Stokes, 2008; Winsborrow and others, 2010; MacGregor and others, 2013). However, shear margins remain under-sampled, in part because they are often heavily crevassed, making ground-based fieldwork difficult.

Lateral shear-margin moraines have been found along paleo-ice streams of the Laurentide and Fenno-Scandinavian ice sheets (Dyke and Morris, 1988; Hodgson, 1994; Kleman and Borgstrom, 1994; Punkari, 1995; Stokes and Clark, 1999, 2002), ranging in width from 250 to 6000 m, with heights of 10–60 m and lengths of 1–70 km. Approximately 30 of these features have been described in publications (Hindmarsh and Stokes, 2008). Here we describe what we believe is the first-ever observation of subglacial bedforms found under the shear margin of an actively flowing ice stream.

We performed an extensive geophysical survey of the bed of the NE Greenland Ice Stream (NEGIS) to diagnose the subglacial properties responsible for its streaming ice flow. In addition to large-scale heterogeneities in bed properties across the ice stream, we found small-scale heterogeneities indicative of subglacial bedforms within the shear margins. Because the survey was designed to broadly characterize subglacial properties (Christianson and others, 2014), the spatial resolution was not optimized to fully characterize bedforms in the subglacial environment. Nonetheless, the data are sufficient to provide useful insights.

Here we detail morphology and material properties of bedforms within the NEGIS shear margins and couple these measurements with remotely sensed observations of ice flow. We perform subglacial water flow modeling to relate observed bedforms to water routing. We additionally model ice infiltration rate into sediments. These combined observations and modeling results then help us place some constraints on the formation mechanism for the observed bedforms.

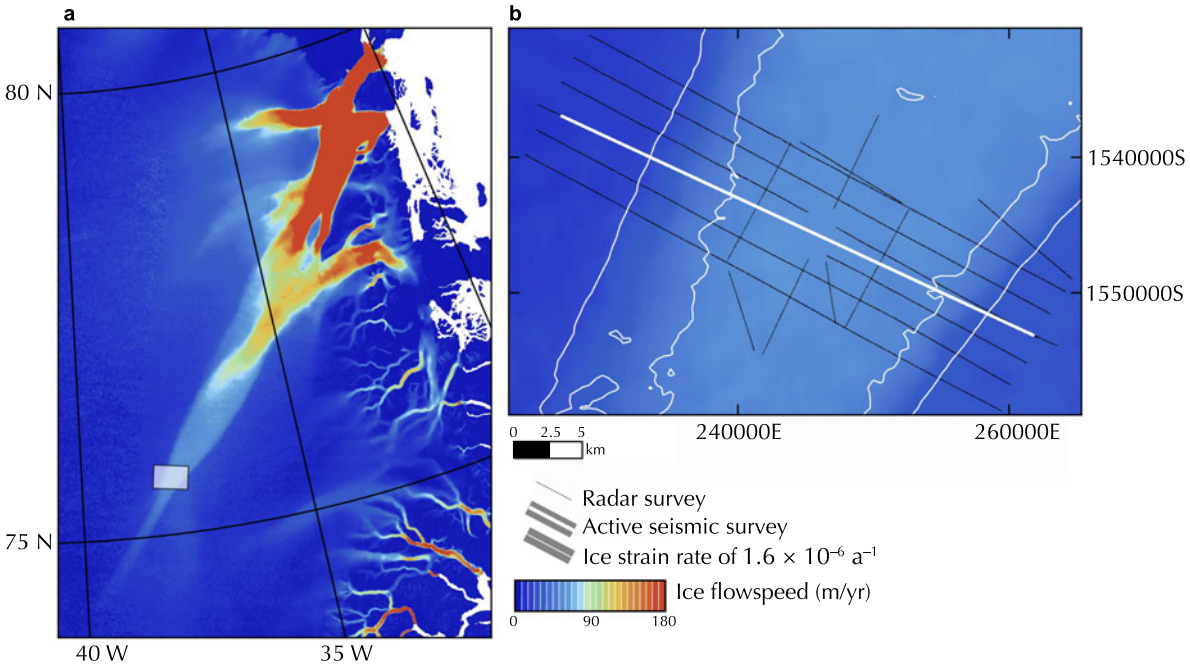

Fig. 1. Ice flowspeed across Greenland from Interferometric Synthetic Aperature Radar (InSAR). (a) NE Greenland Ice Stream study area, indicated with a white box. (b) Geophysical survey at NEGIS. The seismic profile is indicated by the thick white line, and the radar profiles are indicated by the black lines. The ice velocities and strain rates are from 2015 to 2016 Sentinel-1 synthetic aperture radar (Nagler and others, 2015).

Study area

The study area spans the width of the Northeast Greenland Ice Stream (NEGIS), ~140 km downstream from the ice divide (Fig. 1). In the survey area, ice is ~2700 m thick, with flowspeeds of 17–57 ma^{-1} along a transect across-flow (Riverman and others, 2019). This survey is centered on the site that was subsequently selected for the deep ice core of the East Greenland Ice-core Project (EGRIP; http://eastgrip.org/). Figure 1 shows the location of the 2012 geophysical surveying field campaign. Previous work has detailed the associated ground-based ice penetrating radar (GPR; Christianson and others, 2014; Keisling and others, 2014), shallow ice-coring (Vallelonga and others, 2014) and firn thickness observations (Riverman and others, 2019) at this site. The site has distinct shear margins, but the strain rates are low enough that crevassing is not present, allowing for ground-based surveys across the shear margins.

It is unlikely that there is temperate ice within the shear margins in our study area. Elsewhere in Greenland and Antarctica, temperate ice can partially determine ice-stream shear-margin location and stability (Suckale and others, 2014; Perol and others, 2015; Meyer and others, 2018b). However, the low strain rates ($< 5.5 \times 10^{-3}$ a^{-1}) and high degrees of ice incorporation across the shear margins limit temperate ice formation here. This is further supported by GPR surveys across our study area, which do not show any evidence for temperate ice within the shear margins of NEGIS (Christianson and others, 2014; Holschuh and others, 2019).

Methods

We use a combination of geophysical techniques to characterize the subglacial environment across the ice stream. Active seismic surveys were used to determine the material properties of the bed. These results were then paired with a GPR survey to determine the bedform length and geometry. We additionally model subglacial water flow under NEGIS to identify possible regions of well-drained bed and quantify the largest-possible channels within our study area. We later use these values to demonstrate that the observed subglacial features cannot be large meltwater channels.

GPR data were collected across both ice-stream shear margins (Fig. 1). GPR data were acquired using a mono-pulse system operating at a center frequency of 2.5 MHz (Welch and Jacobel, 2003; Christianson and others, 2014). Details of the GPR processing are presented in Christianson and others (2014). Corrections to the data include bandpass filtering, time correction for antenna spacing, interpolation to constant trace spacing, two-dimensional time-wave number migration, time correction for spatially variable firn density and a correction for spherical divergence and englacial attenuation.

We conducted a GPS survey of the ice surface in order to determine the bed elevation from the seismic and radar surveys. GPS data were collected using dual-frequency receivers and processed using differential carrier-phase position as implemented in the Track software (Chen, 1998). Ice-flow direction and shear strain rates were calculated from InSAR-derived ice surface velocities averaged from 1995 to 2013 (Joughin and others, 2010) following eigenvalue-based techniques, detailed in Riverman and others (2019).

Seismic amplitude analysis

Multichannel seismic reflection data of the basal environment were collected along a 38-km transect across both shear margins of the ice stream. One-kg pentolite explosive charges were detonated ~20 m below the surface at the center of and 480 m off one end of a 48 single-component (vertical) geophone array with a 20-m spacing; the geophone array was then moved forward 480 m, and the shooting sequence was repeated, resulting in two-fold seismic data coverage.

We use the measured firn velocity profile of Riverman and others (2019) to correct for firn structure variations across the ice stream. Firn corrections are particularly important for NEGIS because the firn thickness varies dramatically across the shear margins (Christianson and others, 2014; Riverman and others, 2019). The data were further corrected for surface topography and shot depth. We performed frequency filtering, frequency-wavenumber (FK) filtering and normal moveout correction before stacking the data. Finally, the data were migrated

https://doi.org/10.1017/aog.2019.43 Published online by Cambridge University Press

with an ice P-wave velocity of 3700 ms^{-1}. The feature geometries presented below are measured from the migrated seismic sections.

We calculated the bed acoustic impedance (the product of material P-wave velocity and density) across the ice stream based on the amplitude of the seismic reflection from the ice–bed interface to determine the material properties of the ice–bed interface. The processing workflow for the source amplitude corrections started with raw shot data after the bad traces were removed (i.e., no frequency-based filtering was applied to the data in the source amplitude analysis). We restricted the source-receiver offsets used in this analysis to those with angles of incidence less than 10 degrees to minimize the effects of changing bed amplitude with incident angle. We followed the procedures and assumptions of Muto and others (2019) to determine the source amplitude and calculate acoustic impedance at the bed. The source amplitude (A_0) was determined using the direct-path approach of Holland and Anandakrishnan (2009). We chose to use the direct-path approach over the more commonly used multiple-bounce method of Smith and others (2007) because our data lacked strong multiple reflections across most of the ice stream. The path amplitude factor (γ) and primary-ray-path length (d_1) were determined using a one-dimensional velocity model of the glacier that includes both firn and ice (following the procedures of Muto and others, 2019).

We calculated the normal-incidence reflection coefficient, R_0, from the amplitudes of the source and the primary reflection (A_0 and A_1, respectively) as:

$$R_0 = \frac{A_1}{A_0}\frac{1}{\gamma}e^{\alpha d_1} \quad (1)$$

where γ is the path amplitude factor accounting for geometrical spreading and α is the attenuation constant, chosen here as 2.7×10^{-4} m^{-1} (Horgan and others, 2011). That attenuation constant was calculated for ice across the West Antarctic Ice Sheet, which likely has a similar mean annual air temperature as our site near the summit of Greenland. Horgan and others (2011) note that uncertainty in attenuation is the major source of uncertainty in their subsequent seismic amplitude analysis, and this is likely the major source of unquantified uncertainty in our analysis as well.

Of note, there are polarity reversals in A_1 across the ice stream, so R_0 can be positive or negative. We estimate the A_1 and uncertainty for each shot by averaging all available traces within a shot gather and take the standard deviation as the uncertainty.

From R_0 we then calculate the bed acoustic impedance, Z_b (Smith and others, 2007; Luthra and others, 2017):

$$Z_b = Z_{ice}\frac{1+R_0}{1-R_0} \quad (2)$$

where we assume $Z_{ice} = 3.33 \pm 0.04 \times 10^6$ kg m^{-2} s^{-1}, following Atre and Bentley (1993). We estimate the error in Z_b for each shot by propagating the uncertainty in A_0, A_1 and α through Eqns. (1) and (2). This does not account for uncertainty in the attenuation constant. We then use the acoustic impedance of the subglacial material to identify its composition based on the known acoustic impedances of commonly observed subglacial materials. Dilated sediments are generally assumed to have an acoustic impedance range of 2.3×10^6–3.85×10^6 kgm^{-2} s^{-1} (from Atre and Bentley (1993) and also used by Muto and others (2019), Smith (1997) and Brisbourne and others (2017)). Water has an acoustic impedance of 1.49×10^6 kg m^{-2} s^{-1}.

Following Muto and others (2019) we assume that values of $Z_b > 3.85 \times 10^6$ kg m^{-2} s^{-1} correspond to a till porosity of <0.3 and include lodged, non-deforming till. We refer to these regions as 'consolidated sediments,' though they may include sedimentary or crystalline bedrock. Values of 2.3×10^6 kg m^{-2} s^{-1} < Z_b < 3.85×10^6 kg m^{-2} s^{-1} correspond to till that is much softer, deformable and saturated with high-pressure water (Atre and Bentley, 1993; Peters and others, 2007, 2006; Luthra and others, 2017; Muto and others, 2019). See Muto and others (2019) for additional details, uncertainty estimates and a more extensive discussion of this technique for calculating acoustic impedance of subglacial materials.

Modeling water flow

Some studies have related bedform development to fluvial sediment transport (Shaw, 2010). Others have linked variations in effective pressure (the difference between ice overburden pressure and water pressure) with sediment transport and bedform development (Iverson and others, 2017). We model water flow under NEGIS using the Glacier Drainage System (GlaDS) model (Werder and others, 2013) to determine if the bedforms observed under NEGIS form via some fluvial process.

Wet bedforms might share some qualitative characteristics with subglacial channels in geophysical surveys, and subglacial channels are thought to form under some shear margins with high lateral strain rates (Perol and others, 2015; Elsworth and Suckale, 2016; Meyer and others, 2016; Platt and others, 2016). We perform hydrologic modeling to constrain the range of channel sizes and locations for this site. By specifying a very high basal melt rate, we put an upper bound on channel size, which can be compared to observed feature morphology to discriminate between wet sediment and water-filled channels.

GlaDS is a 2-D finite-element model that simulates both distributed and efficient drainage networks beneath the ice. R-channels are modeled along the element edges including creep closure, viscous dissipation of heat and supercooling freeze-on, while the distributed system is modeled across the element with a Darcy–Weisbach type flow equation in the form of linked-cavities or sediment depending on the system conductivity. Water is exchanged between the distributed and channelized systems, which allows the subglacial drainage configuration to evolve over time. Details of the model configuration used here, including the model domain and resolution, can be found in Dow and others (2018). The model domain extends across the entire Greenland Ice Sheet, but is higher-resolution within the NEGIS catchment. Fahnestock and others (2001) found peak melting of >0.1 ma^{-1} in the anomalous region at the head of NEGIS, whereas melt elsewhere beneath the ice sheet is typically 0–0.01 ma^{-1}. We assign a high value of 0.1 ma^{-1} to the entire domain. This provides an end-member estimate of water flux within our study area.

Modeling ice infiltration into sediments

We model the depth of frozen sediments accreted to the bottom of the ice column across the ice stream to test the hypothesis that sediment movement under NEGIS is in part controlled by ice infiltration into the underlying sediments. We use the thermomechanical of Rempel (2008) as implemented by Meyer and others (2018a) and Meyer and others (2019) to calculate the steady-state ice-infiltration depth into the till, h. At the base of ice streams underlain by till, ice can infiltrate into the sediments where pore water pressure is low (and therefore effective stress is high) and where the basal melt rate is low. Where effective pressures are above a critical threshold, P_f, ice intrudes into the interstitial pore spaces (Rempel, 2008; Meyer and others, 2018a, 2019). The model is derived from first

https://doi.org/10.1017/aog.2019.43 Published online by Cambridge University Press

principles and verified experimentally (Rempel and others, 2004; Rempel, 2007, 2008). See Meyer and others (2018a) for an extended discussion of the derivation and use of this model.

The transient problem can be reduced to an idealized one-dimensional second-order partial differential equation for temperature. Properties of the till layer included here are its porosity ϕ, the variation in ice saturation S_i and permeability k with temperature, and the density difference $\Delta\rho_{till}$ between the sediment particles and water ρ. Steady-state infiltration depth satisfies:

$$h \approx \frac{N - p_f - \phi\frac{\rho L}{T_m}\int_{T_f}^{T_l} S_i dT - \eta\dot{m}\int_{z_f}^{z_l}\frac{(1-\phi S_i)^2}{k}dz}{(\rho L/T_m)G + \Delta\rho_{till}(1-\phi)g} \quad (3)$$

where N is effective pressure, η is water viscosity and $\dot{m}$ is the melt rate. The terms in the denominator of Eqn. (3) describe the change in vertical pressure exerted across wetting films and buoyancy of the overlying till with infiltration thickness. The temperature gradient through the ice-infiltrated sediments G is approximated as a constant, 0.03 km^{-1}. The numerator includes terms for the effective stress, N at the base of the ice-infiltrated layer. The second term, $p_f = \rho L(1 - T_f/T_m)$, is the load supported by the wetting films at the base of the ice-infiltrated layer. The final term in the numerator accounts for deviations of the liquid pressure gradient away from hydrostatic equilibrium. Parameter choices here include $\phi = 0.35$, $\Delta\rho_{till} = 1650$ kg m^{-3}, and $T_m - T_f = 0.031$ K, with the ice saturation and permeability modeled using the power laws

$$S_i = 1 - \left(\frac{T_m - T_f}{T_m - T}\right)^{\beta} \quad \text{and} \quad k = k_0\left(\frac{T_m - T_f}{T_m - T}\right)^{\alpha}, \quad (4)$$

with $\beta = 0.53$, $\alpha = 3.1$ and $k_0 = 4.1 \times 10^{-17}$ m^2.

The model is quite sensitive to the selected effective pressure, which is difficult to directly measure. GLaDS models effective pressure across our study area, but the resulting modeled effective pressure variations across the ice stream are perhaps unrealistically low in our study area (−0.2 to 0.3 MPa). Instead, we assume that the shear stress, τ_b, and effective pressure are related at the basal boundary using the Mohr–Coulomb relationship.

$$\tau_b = \mu N \quad (5)$$

where μ is the coefficient of friction, and cohesion is neglected (Iverson and others, 1998; Minchew and others, 2016; Meyer and others, 2019). The coefficient μ is assumed to be 0.6, following Meyer and others (2019). We use the basal shear stress approximation from Holschuh and others (2019), which was inverted for using Elmer/Ice (Zwinger and others, 2007; Gagliardini and others, 2013). We assume a geothermal heat flux of 75 mW m^{-2} from Davies (2013). All of the other model parameter choices follow those of Meyer and others (2019), as detailed in their Table 1.

Results

Acoustic impedance of the subglacial material across NEGIS generally falls into the range of soft, saturated, dilatant sediments (Fig. 2c). There are several bump-like features along the seismic profile that could be interpreted as subglacial bedforms at km 10, 16, 17, and 33 in Figure 2. Here, we use our co-located radar survey to determine which of these possible bedforms extend up- and down-glacier. One feature in the southern shear margin extends across several radar survey lines (Fig. 3). Another feature in the northern shear margin extends across two radar lines. Other candidate bedforms identified from the seismic survey have less-clear upstream–downstream continuation, so they are not discussed further here. However, we note that higher-resolution radar surveys within this study area are likely to find additional streamlined features. Below we detail properties of these margin bedforms and overlying ice and then compare their locations to modeled meltwater flowpaths and ice infiltration depths.

Margin bedforms

The two major subglacial features we identify in the seismic stacked section are labeled with black boxes in Figure 2b. The subglacial bedforms are 40–60 m high (assuming an ice P-wave velocity of 3700 ms^{-1}) and are 400–700 m wide. Near-offset seismic acoustic impedance data (Fig. 2c) show that each marginal bedform is composed of soft, water-saturated till.

Coincident radargrams from Christianson and others (2014) show undulations in the bed that correspond with the seismically identified soft, deformable bedforms (Fig. 2). Radar profiles upstream and downstream of the seismic survey provide constraints on the length of features, although the length estimates are limited by the along-flow spacing of our radar lines (Figs 3 and 4).

The feature in the southern shear margin is one ice thickness instream of the location of maximum strain rate. It is 670 m wide and 62 m tall (inferred from the migrated seismic and radar surveys). It is likely visible across five of our radar transects, indicating that it is ~6.6 km long. We do not seismically detect any large internal reflectors within the bedform. This suggests that the bedform is composed of homogeneous till with no major variations in density or seismic velocity. The acoustic impedance of at least the upper few meters of the feature is quite low: $\sim 3.1 \times 10^6$ kg m^{-2} s^{-1}, indicating high-porosity, water-saturated till. On the south side of the feature, the bed transitions to stronger material with a higher acoustic impedance ($\sim 4.6 \times 10^6$ kg m^{-2} s^{-1}) within 500 m of the bedform. We find no such boundary on the northwest side of the bedform (toward the center of the ice stream). Figure 5 shows the location of the bedform relative to ice-flow direction and shear margin position. The bedform is roughly flow-parallel, and ice-flow velocity increases significantly along the length of the feature as the ice enters the ice stream: from 29.5 ma^{-1} at the most upglacier radar line to 51.9 ma^{-1} at the most downglacier radar line.

The feature in the northern shear margin is 1 km outboard of the point of maximum strain rate. The acoustic impedance of the feature is $\sim 3.1 \times 10^6$ kg m^{-2} s^{-1}, indicating high-porosity, water-saturated till. This is the same acoustic impedance as the bedform in the southern shear margin. Where crossed by the seismic survey, the bedform is 410 m wide and 44 m tall. It is visible in two of our radar transects, indicating that it is at most 5.1 km long. There are no prominent internal reflectors within this bedform, suggesting that it is composed of homogeneous till with no major increases in acoustic impedance at the resolution of our seismic survey. The feature is in a broad region of low acoustic impedance, where soft deforming sediments are pervasive. Ice flowspeed does not change significantly along the length of the feature, with flowspeeds of ~39 ma^{-1}. This feature is roughly flow-parallel (see Fig. 5).

Radar brightness across the subglacial features (presented in Christianson and others, 2014, but not detailed further here) is varied, with no clear pattern. However, we would not expect to see a strong correlation between seismic and radar reflection strength across features because of differences in the resolution of the systems as well as differences in the physical features of the subglacial environment that result in reflections. We also

https://doi.org/10.1017/aog.2019.43 Published online by Cambridge University Press

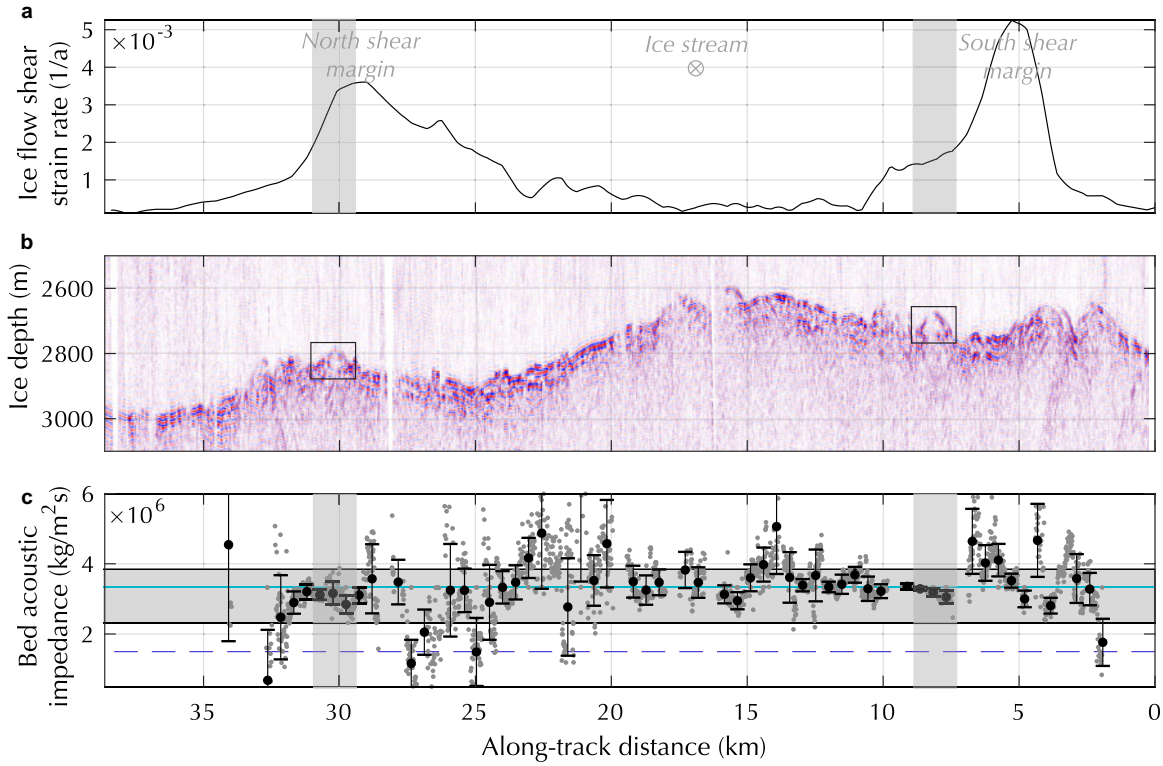

Fig. 2. Subglacial conditions across the NE Greenland Ice Stream from active seismic data. The location in Greenland is shown as the white line in Figure 1b. Gray vertical bands correspond to the subglacial features described in the text. Ice flow within the ice stream is into the page. The features discussed in the text are shown with black boxes. (a) Strain rate across the ice stream resulting from ice flow (Riverman and others, 2019), as measured from Interferometric Synthetic Aperture Radar (Joughin and others, 2010). (b) Stacked, unmigrated seismic section showing the basal reflector. The black boxes indicate bedforms described here. Figures 3 and 4 show enlargements of these areas and coincident radargrams. Additional bumps (e.g., at km 17) may be bedforms but are not observed clearly in parallel radar lines upstream or downstream. (c) Acoustic impedance of the subglacial materials, Z_B, for each receiver (gray dots) and shot-averaged (black dots). Error bars show one standard deviation of variance for measurements in each shot. Horizontal lines show modeled acoustic impedances for common subglacial materials. The cyan line shows the acoustic impedance of ice. The blue dashed line shows the acoustic impedance of water. Black lines and the filled gray box show values of 2.2×10^6 kg m^{-2} s$^{-1} < Z_b < 3.8 \times 10^6$ kg m^{-2} s^{-1} correspond to soft, deformable, water-saturated till (Atre and Bentley, 1993; Smith, 1997).

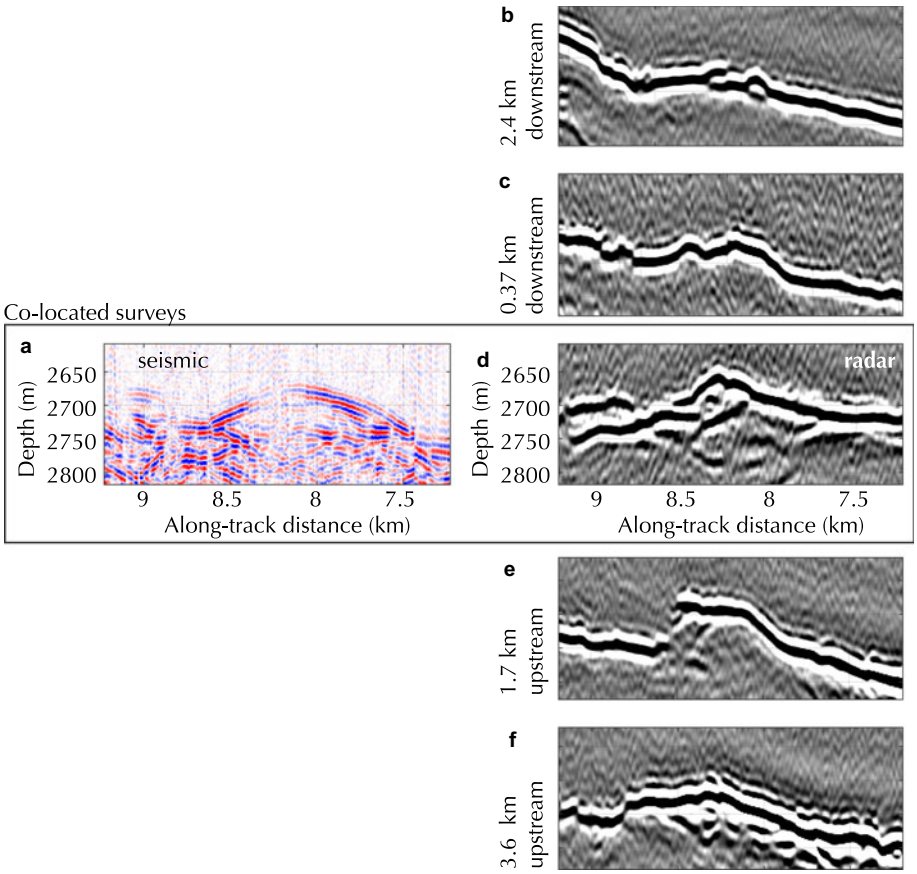

Fig. 3. Seismic and radar lines showing the bed reflector across the southern shear margin of the NE Greenland Ice Stream. Location of the picked bedform is shown in Figure 2. Distances upstream/downstream are relative to the bedform at the seismic line. (a) Active seismic line across the bedform. (b) Radar line 2.4 km downstream from seismic line. (c) Radar line 0.34 km downstream from seismic line. (d) Radar line co-located with seismic line. (e) Radar line 1.7 km upstream of seismic line. (f) Radar line 3.6 km upstream of seismic line. For (b)–(f), the *X* and *Y* axes have the same scale as those noted for (d), with slightly shifted positions to center the feature.

https://doi.org/10.1017/aog.2019.43 Published online by Cambridge University Press

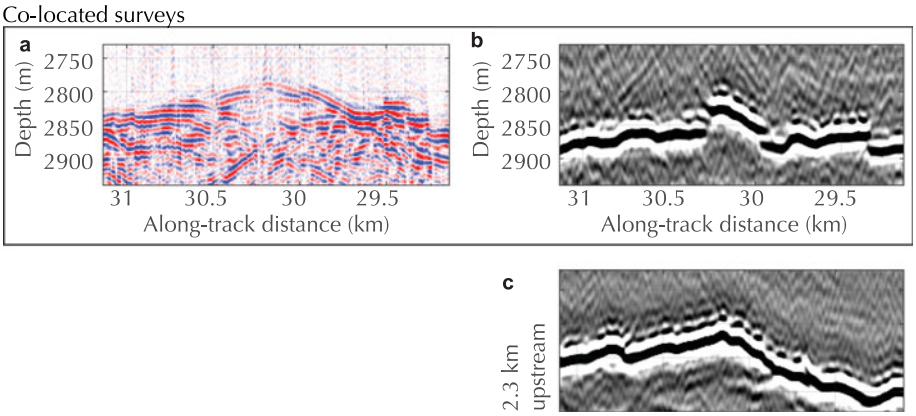

Fig. 4. Seismic and radar lines showing the bed reflector across the northern shear margin of the NE Greenland Ice Stream. Location of the picked bedform is shown in Figure 5. (a) Active seismic line. (b) Radar line co-located with seismic line. (c) Radar line 2.3 km downstream from seismic line. For (c), the *X* and *Y* axes have the same scale as those noted for (b), with a slightly shifted position to center the feature.

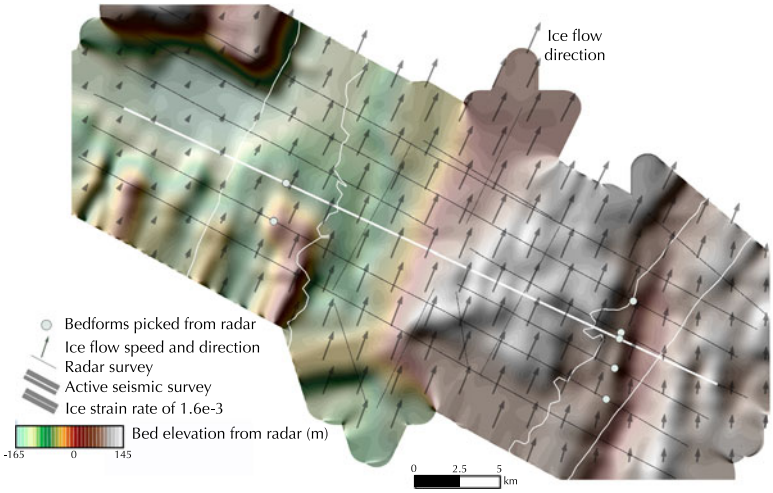

Fig. 5. Map of bed elevation showing picked bedforms (green dots), ice-flow direction (gray arrows, with size indicating flowspeed from 9 to 51 ma^{-1}), seismic survey (white thick line), and radar survey (gray thin line). Areas bounded by the thin white line show where the ice-flow strain rate is greater than $1.6e^{-3}$ a^{-1}. Site location corresponds to the inset in Figure 1a and covers the same region as Figure 1b.

note that these features are very close to the horizontal resolution of the radar system: the Fresnel zone of the 2.5 MHz radar system is 416 m (using an electromagnetic wave velocity of 170 m(u s)$^{-1}$) and 312 m for the seismic system (using a P-wave velocity of 3700 ms^{-1} and a seismic frequency of 100 Hz). Additionally, the seismic data have a higher vertical resolution, with a theoretical (1/4 wavelength) resolution of 9.25 m, compared to the 17 m vertical resolution of the radar system. As such, we do not expect the radar reflection brightness to mimic the patterns of acoustic impedances reported here.

Meltwater routing and sediment-entrained ice depth

The GLaDS subglacial hydrology model results show that even under end-member high melt rates, much of the water movement through this region is within the distributed system. Only limited regions of continuous channelization are observed in model results. The greatest degree of channelization occurs in the shear margins of the ice stream (Fig. 6b), consistent with previous water-routing studies (Karlsson and Dahl-Jensen, 2015). The water flow modeling work shown here provides no evidence for the role of water movement in bedform development. The location of strongest discharge and channelization does not correlate with bedform location (Fig. 6b). However, the bedforms described here have too large of a cross-sectional area (>7000 m^2) to be Rothlisberger channels.

We have also modeled the steady-state ice-infiltration depths across the ice stream. Model results show that debris-rich ice depth decreases as ice crosses the shear margin and flows into the ice stream (Fig.6c). As modeled effective pressures decrease along flowlines moving into the ice stream, basal ice layers may melt and deposit sediments. In the southern shear margin, the location of the bedform (km 8 in Fig. 6) corresponds with the location where modeled steady-state ice infiltration depths first decrease, suggesting that sediment is 'dropped' or melted out of the ice column. In the north shear margin, the bedform is also in a broad region where modeled sediments are being deposited from the overlying ice column.

Discussion

Our results show two possible bedforms beneath the NEGIS shear margins. These bedforms are composed of soft, deformable, water-saturated sediments. Other features are visible in the seismic section that may be bedforms, but in the absence of higher-resolution radar data, we are reticent to speculate on their properties.

The size and location of Feature 1 in the southern shear margin are similar to those of features that Stokes and Clark (2002) classified as ice stream margin moraines, and correspond most closely to the lateral shear moraines of Batchelor and Dowdeswell (2016). We thus conclude that this is a lateral shear moraine. To the best of our knowledge, this is the first subglacial observation of such a feature. This feature can provide insights into the ice-flow processes necessary to form the lateral shear moraines of previously glaciated landscapes.

Possible formation mechanism

There is little consensus on a universal formation model for marginal moraines, though many have been proposed (as

https://doi.org/10.1017/aog.2019.43 Published online by Cambridge University Press

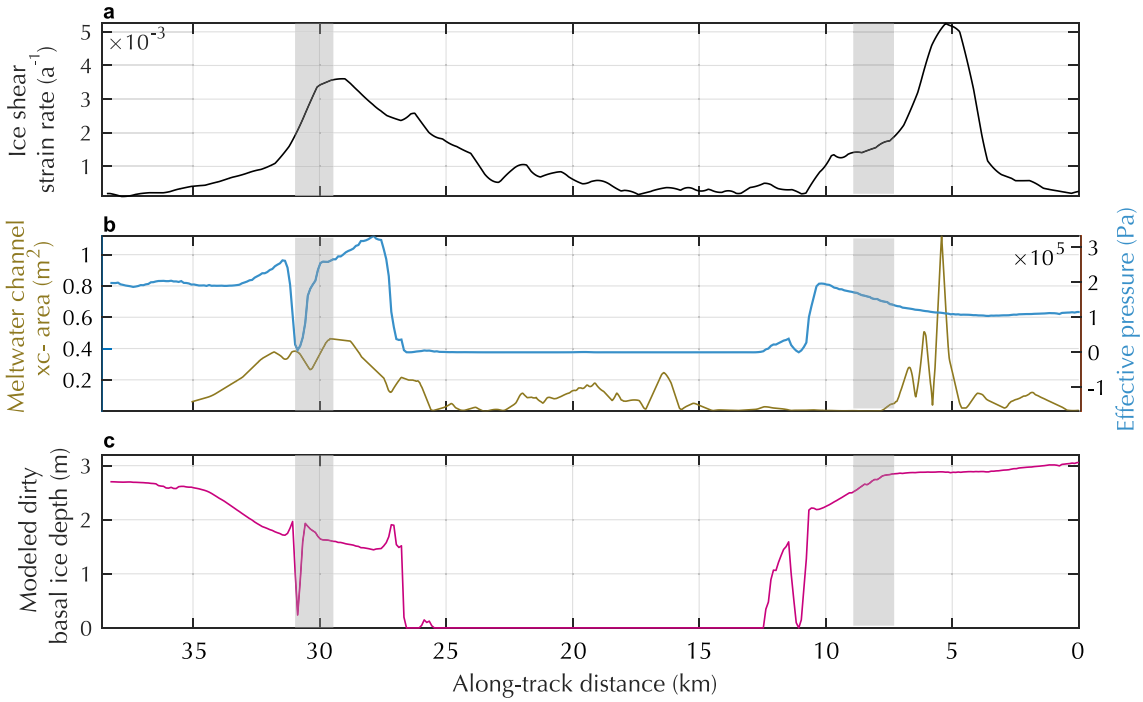

Fig. 6. Modeled meltwater flow across NEGIS. Gray bands indicate the location of bedforms presented here. (a) Location of the NEGIS shear margins, from the ice-flow strain rate. (b) The left axis and yellow line show meltwater channel cross-sectional area from GLaDS modeling. The right axis shows effective pressure at the same locations, as calculated from an ice-flow modeling inversion for basal shear stress. (c) Modeled ice infiltration depth into sediments (forming dirty basal ice layers) using the effective pressures presented in pannel b.

summarized in Stokes and Clark, 2002; Hindmarsh and Stokes, 2008). These features may form through a similar mechanism to drumlins and mega-scale glacial lineations within the ice stream; however, this does not explain their preferential formation within the shear margins nor their size differences from features found within regions of fast flowing ice (marginal features are generally wider and longer (Batchelor and Dowdeswell, 2016)). For this reason, we focus here on formation mechanisms unique to the shear margins. Below we briefly summarize several previously proposed marginal moraine formation mechanisms and address their relevance to our observations. We then put forward our preferred theory by which sediment that is well-coupled with and entrained in basal ice melts out within the shear margins.

Shear marginal moraines may form at the boundary between warm-based and cold-based ice, arising from thermally controlled differences in erosion rate (Dyke and Morris, 1988; Kleman and Borgstrom, 1994). This model is unlikely to be relevant for NEGIS. Our data, as well as those synthesized by MacGregor and others (2016), show a thawed bed under the ice stream and outside the shear margin to the south, so a thermal boundary cannot be important for the southern shear margin bedform. Regional analysis shows the possibility of a frozen bed outside of the northern margin (MacGregor and others, 2016), but Christianson and others (2014), Holschuh and others (2019), and this study have found evidence for subglacial water in the region. Thus, we conclude that these marginal bedforms did not form because of the effect of thermal boundaries on subglacial erosion rates. We also note that it is unlikely that the thermal regime of this area has recently shifted (Keisling and others, 2014).

Elsewhere, shear margin moraines have been found co-located with a topographic step (with the core of ice stream flow sitting 40 m below the surrounding topography) (Stokes and Clark, 2002) suggesting that till is excavated from within the ice stream and deposited in the margins. We find no such topographic step across the ice stream (Fig.5), so the source of the till within the marginal bedforms could be external to the ice stream, and there is no clear evidence to support the model that till is excavated from the ice stream interior and deposited within the shear margins.

Shear marginal moraines may also form in regions of ice flow compression or ablation. Hindmarsh and Stokes (2008) present a quantitative model where the ice stream lateral moraines are formed via differential erosion rates related to lateral variations in the ice stream velocity. In their model, subglacial till deposition occurs where there is surface ablation or compressing flow. At NEGIS, we are well within the accumulation zone so would not expect till deposition due to surface ablation. Additionally, the bedforms observed here are within regions of extensional flow (as shown in Fig. 7b of Riverman and others (2019)). As a result, from the Hindmarsh and Stokes model (2008) we would expect slight erosion of till within the shear margins of NEGIS.

Alternatively, we hypothesize that ice–till coupling across the shear margins and ice infiltration into the sediments collectively contribute to the deposition of sediments within the shear margins of NEGIS. Strong coupling between ice and sediment favors till deformation, whereas decoupling across ice-contact water favors rapid basal motion but reduced till deformation (e.g., Iverson and others, 1995; Fischer and Clarke, 2001). The strong velocity variations seen across this area suggest that there are changes in subglacial effective pressure, with areas of low effective pressure lubricating fast ice flow. As ice flows across the shear margins on NEGIS, effective pressure drops and the degree of ice–till coupling likely decreases, resulting in till deposition in the shear margins. Similarly, ice infiltration into sediments varies with changing effective pressures. Figure 6b shows our estimates for effective pressure across the ice stream assuming the Mohr–Coulomb relationship. Ice can infiltrate into sediments where the effective pressures are high (Rempel, 2008; Meyer and others, 2018a). These sediments can later be deposited as the effective pressures decrease and more rapid basal sliding initiates. Our ice-infiltration depth modeling efforts show that the location of observed subglacial bedforms corresponds to locations where we would expect to see sediments accumulating due to decreases in ice-infiltration depth.

https://doi.org/10.1017/aog.2019.43 Published online by Cambridge University Press

A similar theoretical model has been previously applied to the formation of drumlins at Múlajökull, Iceland (Iverson and others, 2017). Sediments there are thought to be entrained in the basal ice at the head and flanks of drumlins during quiescent flow due to high effective pressures. During surge events, subglacial effective pressures drop, sediments are deposited and the drumlins migrate downglacier. Here, we propose a similar model of sediment movement via variations in effective pressure. However, instead of temporal variations in effective pressure driving sediment movement, we propose that spatial variations in effective pressure are responsible for the differential till erosion and deposition rates.

Our hypothesis for bedform formation within the shear margins could explain why shear marginal bedforms are relatively rare across the paleo-record: we would expect to see them form only where there is strong ice-flow advection across ice stream shear margins (i.e., at locations where the ice stream is widening) and where there are strong variations in effective pressure across the shear margin.

It is difficult to fully propose a theory for the formation of these ice stream margin features without higher-resolution geophysical data to constrain their geometries. We find it likely that effective pressure variations, which drive differential entrainment and transport rates, are at play, but we currently have little means to test this hypothesis further.

Conclusions

Our geophysical surveys across the North East Greenland Ice Stream (NEGIS) reveal what we believe to be the first shear margin moraine observed under a margin of an active ice stream. This offers a valuable laboratory for future study of the formation and evolution of these enigmatic features of the paleo-record.

The observed bedforms are composed of saturated, soft, high-porosity till with a low acoustic impedance, and the orientation of the features is flow-parallel. We hypothesize that bedforms are the result of preferential deposition of till within the shear margins resulting from variable till coupling and ice infiltration into sediments. Future modeling and observational work are necessary to more completely describe the formation of the basal features across the shear margins of NEGIS.

Acknowledgments. K.R. was supported by the National Science Foundation Graduate Research Fellowship under Grant No. DGE1255832, with additional funding from the University of Oregon Department of Earth Sciences. K.C. was supported by NASA grant NNX16AM01G. C.D. was supported through Natural Sciences and Engineering Research Council of Canada (RGPIN-03761-2017) and Canada Research Chairs Program (950-231237). B.R.P. was supported by NASA grant NNX15AH84G and NSF grants PLR-1443190 and AGS-1338832; R.B.A. acknowledges support from PLR-1738934. All authors except C.D. received support from NSF grant OPP-0424589. Logistical support was provided by CH2MHILL Polar Services, the New York Air National Guard, Kenn Borek Air, the Alfred Wegener Institute for Polar and Marine Research, and the North Greenland Eemian Ice Drilling Project. Thank you to C. Meyer and A. Rempel for many useful conversations and comments on the manuscript. All data presented here are available upon request of the corresponding author.

References

Atre SR and Bentley CR (1993) Laterally varying basal conditions beneath Ice Streams B and C. *Journal of Glaciology* **133**, 507–514.

Batchelor CL and Dowdeswell JA (2016) Lateral shear-moraines and lateral marginal-moraines of paleo-ice streams. *Quaternary Science Reviews* **151**, 1–26.

Brisbourne AM and 8 others (2017) Bed conditions of pine island glacier, west antarctica. *Journal of Geophysical Research: Earth Surface* **122**(1), 419–433.

Chen G (1998) *GPS Kinematic Positioning for Airborne Laser Altimetry at Long Valley* (PhD thesis). Massachusetts Institute of Technology.

Christianson K (2014) Dilatant till facilitates ice-stream flow in northeast Greenland. *Earth and Planetary Science Letters* **401**, 1–17.

Clark C (2010) Emergent drumlins and their clones: from till dilatancy to flow instabilities. *Journal of Glaciology* **51**, 1011–1025.

Clarke TS, Liu C, Lord NE and Bentley CR (2000) Evidence for a recently abandonded shear margin adjacent to ice stream B2, Antarctica, from ice-penetrating radar measurements. *Journal of Geophysical Research* **105**, 409–422.

Davies JH (2013) Global map of solid earth surface heat flow. *Geochemistry, Geophysics, Geosystems* **14**(10), 4608–4622.

Dow CF, Karlsson NB and Werder MA (2018) Limited impact of subglacial supercooling freeze-on for Greenland Ice Sheet stratigraphy. *Geophyiscal Research Letters* **45**, 1481–1489.

Dyke A and Morris T (1988) Drumlin fields, dispersal trains, and ice streams in Arctic Canada. *Canadian Geographer* **32**, 86–90.

Elsworth CW and Suckale J (2016) Rapid ice flow rearrangement induced by subglacial drainage in West Antarctica. *Geophyiscal Research Letters* **43**(22), 11697–11707.

Fahnestock MA and 5 others (2001) Ice-stream-related patterns of ice flow in the interior of northeast Greenland. *Journal of Geophysical Research: Solid Earth* **106**(D24), 34035–34045.

Fischer UH and Clarke GKC (2001) Review of subglacial hydromechanical coupling: Trapridge Glacier, Yukon Territory, Canada. *Quaternary International* **86**(1), 29–43.

Gagliardini O and 9 others (2013) Capabilities and performance of elmer/ice, a new-generation ice sheet model. *Geoscientific Model Development* **6**(4), 1299–1318.

Hindmarsh RCA and Stokes CR (2008) Formation mechanisms for ice-stream lateral shear margin moraines. *Earth Surface Processes and Landforms* **33**(4), 610–626.

Hodgson D (1994) Episodic ice streams and ice shelves during retreat of the northwesternmost sector of the Late Wisconsinan Laurentide Ice Sheet over the central Canadian Arctic archipelago. *Boreas* **23**, 14–28.

Holland CW and Anandakrishnan S (2009) Subglacial seismic reflection trategies when source amplitude and medium attenuation are poorly known. *Journal of Glaciology* **55**(193), 931–937.

Holschuh N, Lilien D and Christianson K (2019) Thermal weakening, convergent flow, and vertical heat transport in the Northeast Greenland Ice Stream shear margins. *Geophysical Research Letters* **47**, 1–10.

Horgan HJ, Anandakrishnan S, Alley RB, Burkett PG and Peters LE (2011) Englacial seismic reflectivity: imaging crystal-orientation fabric in West Antarctica. *Journal of Glaciology* **57**(204), 639–650.

Iverson NR and 6 others (2017) A theoretical model of drumlin formation based on observations at mulajokull, iceland. *JGR Earth Surface* **122**(12), 2302–2323.

Iverson NR, Hanson B, Hooke RL, Jansson P (1995) Flow mechanism of glaciers on soft beds. *Science (New York, N.Y.)* **267**(5194), 80–81.

Iverson NR, Hooyer TS and Baker RW (1998) Ring-shear studies of till deformation: Coulomb-plastic behavior and distributed strain in glacier beds. *Journal of Glaciology* **44**(148), 634–642.

Joughin I, Smith BE, Howat IM, Scambos T and Moon T (2010) Greenland flow variability from ice-sheet-wide velocity mapping. *Journal of Glaciology* **56**(197), 415–430.

Karlsson N and Dahl-Jensen D (2015) Response of the large-scale subglacial drainage system of Northeast Greenland to surface elevation changes. *The Cryosphere* **9**(4), 1465–1479.

Keisling BA and 8 others (2014) Basal conditions and ice dynamics inferred from radar-derived internal stratigraphy of the Northeast Greenland Ice Stream. *Annals of Glaciology* **55**(67), 127–137.

King EC, Hindmarsh RCA and Stokes CR (2009) Formation of mega-scale glacial lineations observed beneath a West Antarctic ice stream. *Nature Geoscience* **2**(8), 585–588.

King EC, Pritchard H and Smith AM (2016) Subglacial landforms beneath Rutford Ice Stream, Antarctica: detailed bed topography from ice-penetrating radar. *Earth System Science Data* **8**, 151–158.

Kleman J and Borgstrom I (1994) Glacial landforms indicative of a partly frozen bed. *Journal of Glaciology* **40**(135), 255–264.

Luthra T and 5 others (2017) Characteristics of the sticky spot of Kamb Ice Stream, West Antarctica. *Journal of Geophysical Research: Earth Surface* **122**(3), 641–653.

MacGregor J and 7 others (2013) Weak bed control of the eastern shear margin of Thwaites Glacier, West Antarctica. *Journal of Glaciology* **59**(217), 900–912.

MacGregor J and 11 others (2016) A synthesis of the basal thermal state of the Greenland Ice Sheet. *Journal of Geophysical Research* **121**, 1328–1350.

https://doi.org/10.1017/aog.2019.43 Published online by Cambridge University Press

Menzies J (1989) Drumlins - products of controlled or uncontrolled glaciodynamic response. *Quaternary Science Reviews* **8**, 151–158.

Meyer CR, Downey AS and Rempel AW (2018*a*) Freeze-on limits bed strength beneath sliding glaciers. *Nature Communications* **9**(3242), 1–6.

Meyer CR, Fernandes MC, Creyts TT and Rice JR (2016) Effects of ice deformation on Röthlisberger channels and implications for transitions in subglacial hydrology. *Journal of Glaciology* **62**(234), 750–762.

Meyer CR, Robel AA and Rempel AW (2019) Frozen fringe explains sediment freeze-on during heinrich events. *Earth and Planetary Science Letters* **524**, 115725.

Meyer CR, Yehya A, Minchew B and Rice JR (2018*b*) A model for the downstream evolution of temperate ice and subglacial hydrology along ice stream shear margins. *Journal of Geophysical Research: Earth Surface* **123**, 1682–1698.

Minchew B and 7 others (2016) Plastic bed beneath hofsjökull ice cap, central iceland, and the sensitivity of ice flow to surface meltwater flux. *Journal of Glaciology* **62**(231), 147–158.

Muto AM and 7 others (2019) Relating bed character and subglacial morphology using seismic data from Thwaites Glacier, West Antarctica. *Earth and Planetary Science Letters* **507**, 199–206.

Nagler T, Rott H, Hetzenecker M, Wuite J and Potin P (2015) The Sentinel-1 mission: new opportunities for ice sheet observations. *Remote Sensing* **7**, 9371–9389.

Perol T, Rice J, Platt J and Suckale J (2015) Subglacial hydrology and ice stream margin locations. *Jounral of Geophysical Research* **120**(7), 1352–1368.

Peters LE (2006) Subglacial sediments as a control on the outset and location of two Siple Coast ice streams, West Antarctica. *Journal of Geophysical Research* **111**, 1–14.

Peters LE, Anandakrishnan S, Alley RB and Smith AM (2007) Extensive storage of basal meltwater in the onset region of a major West Antarctic ice stream. *Geology* **35**(3), 251–254.

Platt JD, Perol T, Suckale J and Rice JR (2016) Determining conditions that allow a shear margin to coincide with a Röthlisberger channel. *Journal of Geophysical Research: Earth Surface* **121**, 1273–1294.

Punkari M (1995) Function of the ice streams in the Scandinavian Ice Sheet: analysis of glacial geological data from southwestern Finland. *Transactions of the Royal Society of Edinburgh, Earth Sciences* **85**, 283–302.

Rempel A (2007) Formation of ice lenses and frost heave. *Journal of Geophysical Research: Earth Surface* **112**(F2), 1–17.

Rempel AW (2008) A theory for ice-till interactions and sediment entrainment beneath glaciers. *Journal of Geophysical Research* **113**, 1–20.

Rempel AW, Wettlaufer J and Worster MG (2004) Premelting dynamics in a continuum model of frost heave. *Journal of Fluid Mechanics* **498**, 227–244.

Riverman KR and 7 others (2019) Enhanced firn densification in high-accumulation shear margins of the NE Greenland Ice Stream. *Journal of Geophysical Research: Earth Surface* **124**(2), 365–382.

Shaw J (2010) In defence of the meltwater (megaflood) hypothesis for the formation of subglacial bedform fields. *Journal of Quaternary Science: Published for the Quaternary Research Association* **25**(3), 249–260.

Smith A (1997) Basal conditions on rutford ice stream, west antarctica, from seismic observations. *Journal of Geophysical Research: Solid Earth* **102**(B1), 543–552.

Smith A and 6 others (2007) Rapid erosion, drumlin formation, and changing hydrology beneath an Antarctic ice stream. *Geology* **35**(2), 127–130.

Stokes C and Clark C (1999) Geomorphological criteria for identifying Pleistocene ice streams. *Annals of Glaciology* **28**, 67–75.

Stokes CR and Clark CD (2002) Ice stream shear margin moraines. *Earth Surface Processes and Landforms* **27**(5), 547–558.

Suckale J, Platt JD, Perol T and Rice JR (2014) Deformation-induced melting in the margins of the West Antarctic ice streams. *Journal of Geophysical Research: Earth Surface* **116**(5), 1004–1025.

Vallelonga P and 22 others (2014) Initial results from geophysical surveys and shallow coring of the Northeast Greenland Ice Stream (NEGIS). *The Cryosphere* **8**(4), 1275–1287.

Van der Veen C, Jezek K and Stearns L (2007) Shear measurements across the northern margin of Whillans Ice Stream. *Journal of Glaciology* **53** (180), 17–29.

Welch B and Jacobel R (2003) Analysis of deep-penetrating radar surveys of West Antarctica, US-ITASE 2001. *Geophysical Research Letters* **30**(8), 1444.

Werder MA, Hewitt IJ, Schoof CG and Flowers GE (2013) Modeling channelized and distributed subglacial drainage in two dimensions. *Journal of Geophysical Research: Earth Surface* **118**(4), 2140–2158.

Winsborrow M, Clark C and Stokes C (2010) What controls the location of ice streams. *Earth Science Reviews* **103**(1–2), 45–59.

Zwinger T, Greve R, Gagliardini O, Shiraiwa T and Lyly M (2007) A full stokes-flow thermo-mechanical model for firn and ice applied to the gorshkov crater glacier, kamchatka. *Annals of Glaciology* **45**, 29–37.

https://doi.org/10.1017/aog.2019.43 Published online by Cambridge University Press